



# Modeling an alkaline electrolysis cell through reduced-order and loss-estimate approaches



Jaroslaw Milewski<sup>a</sup>, Giulio Guandalini<sup>b</sup>, Stefano Campanari<sup>b,\*</sup>

<sup>a</sup> Institute of Heat Engineering, Warsaw University of Technology, 21/25 Nowiejska Street, 00-665 Warsaw, Poland

<sup>b</sup> Politecnico di Milano, Department of Energy, Via Lambruschini 4, 20156 Milano, Italy

## HIGHLIGHTS

- Modeling of alkaline electrolysis cells.
- Setup of a reduced order equivalent circuit model.
- Setup of a loss estimation model.
- Comparison with experimental data on real alkaline electrolyzer.
- Model accuracy within 3%, adequate for use in complex system analysis.

## ARTICLE INFO

### Article history:

Received 12 December 2013

Received in revised form

13 June 2014

Accepted 18 June 2014

Available online 7 July 2014

### Keywords:

Alkaline electrolysis

Modeling

Experimental analysis

Equivalent circuit

Loss calculation

Electrolyzer

## ABSTRACT

The paper presents two approaches to the mathematical modeling of an Alkaline Electrolyzer Cell. The presented models were compared and validated against available experimental results taken from a laboratory test and against literature data. The first modeling approach is based on the analysis of estimated losses due to the different phenomena occurring inside the electrolytic cell, and requires careful calibration of several specific parameters (e.g. those related to the electrochemical behavior of the electrodes) some of which could be hard to define. An alternative approach is based on a reduced-order equivalent circuit, resulting in only two fitting parameters (electrodes specific resistance and parasitic losses) and calculation of the internal electric resistance of the electrolyte. Both models yield satisfactory results with an average error limited below 3% vs. the considered experimental data and show the capability to describe with sufficient accuracy the different operating conditions of the electrolyzer; the reduced-order model could be preferred thanks to its simplicity for implementation within plant simulation tools dealing with complex systems, such as electrolyzers coupled with storage facilities and intermittent renewable energy sources.

© 2014 Published by Elsevier B.V.

## 1. Introduction

Hydrogen-based technologies promise ultra high efficiency in power generation (up to 65% for Higher Heating Value (HHV) as the reference based on fuel cells [1]) and virtually without environmental impact [2]. Fuel cells are predicted to be efficient sources of combined heat and power in small scale applications [3,4] and are the primary choice for future hydrogen-based mobility [5]. There are several types of fuel cells, of which the most important nowadays are Polymer Exchange Membrane Fuel Cells [6,7], Solid Oxide Fuel Cells [8,9] and Molten Carbonate Fuel Cells [10,11], all of

which are suitable for use with hydrogen [12] which is especially required for the low temperature types. In addition to this, hydrogen is considered a promising way for setting up large scale energy storage facilities suitable for improving the electric grid stability against the power production oscillations of intermittent renewable plants like solar and wind power plants. Thus, efficient and large scale hydrogen generation is very desirable technology [13–15]. Water electrolysis is a well-known process and is currently adopted in many applications in order to produce hydrogen with high purity. The opportunity to connect this technology directly with renewable energy sources has, for instance, led to many studies developing island-oriented storage systems that couple an electrolyzer, local hydrogen storage and a fuel cell to obtain a fully autonomous and controlled power plant based on solar or wind power. Several studies are also addressing hydrogen production

\* Corresponding author.

E-mail address: [stefano.campanari@polimi.it](mailto:stefano.campanari@polimi.it) (S. Campanari).

from fluctuating renewable sources for direct injection into natural gas infrastructures (the so-called power-to-gas concept), where fast-response, high pressure electrolysis is the technology required for hydrogen generation [16].

Various technologies for water electrolysis are currently available or under development. Two electrodes, on which the dissociation reaction of water takes place, and an interposed electrolyte, which allows the transport of distinctive ionic species, are common features of all of them. On the other hand, the nature of the electrolyte brings with it different conceptual operating principles and designs. The most commonly used electrolyte materials are:

- liquid solutions of alkaline hydroxides (usually KOH or NaOH) [14]
- polymer exchange membranes (PEM) [17,18]
- solid oxides [19,20]

Alkaline and PEM electrolyzers usually work in a range of temperatures between 60 and 80 °C. Solid oxide electrolytes need much higher temperatures to be active (600–900 °C); this is a limit referring to the prospect of intermittent operation, at least if a fast thermal transient capability is required, but it increases the fraction of energy required by the dissociation process that can be supplied as heat instead of electricity [21].

While Alkaline and PEM technologies are commercial solutions, solid oxides technology is still at a developmental stage. More precisely, alkaline electrolyzers are a mature technology in industrial applications and a wide number of large units are in operation, while PEMs presently have significant but limited applications in terms of production capacity and still present some issues in terms of lifetime. Nevertheless, much of the research effort is focused on PEMs, looking to avoid the use of a corrosive electrolyte and possibly to an easier increase in operating pressure and a less problematic intermittent operation. The alkaline process is studied with the aim of improving performance in terms of operating pressure, temperature and efficiency, with advantages in terms of proven feasibility on large scales [14].

In this work we focus only on the models related to alkaline technology, due to the prospect of modeling high power electrolyzers working on an intermittent regime with fast load ramps and easy startup/shutdown procedures that cannot be followed by high temperature devices.

In addition to the type of electrolyte, other design parameters that distinguish different electrolyzer technologies are the position and electrical connection scheme of the electrodes.

An alkaline electrolyzer can be traditionally designed with a gap between the electrodes and the interposed separation membrane, which is necessary to avoid the risk of a dangerous mix of hydrogen and oxygen, which are produced on opposite electrodes. In this solution the electrolyte and the products circulate between the electrodes. An alternative and more modern design is based on “zero-gap” cells (see Fig. 1), where the electrodes are pressed on the membrane, allowing an increase in efficiency ([22,23]). Electrolyte and gases permeate the electrodes and are collected on the other side.

As far as the electrical scheme is concerned, cells can be connected in parallel leading to “monopolar” electrolyzers; this choice is simpler to realize and more robust, but needs more complex external connections and circuits, bringing about higher losses. The alternative is a series connection that makes it possible to manufacture the electrodes of two adjacent cells on the two sides of the same plate (“bipolar” electrolyzers — Fig. 2). The resulting component (stack) is more compact; on the other hand parasitic currents have more possible paths and it becomes impossible to set up modular maintenance of single cells without disassembling the whole stack.

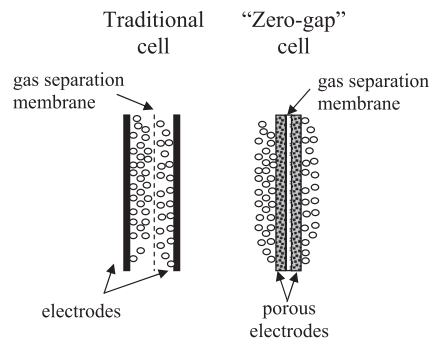


Fig. 1. A “zero-gap” design of alkaline electrolyzer.

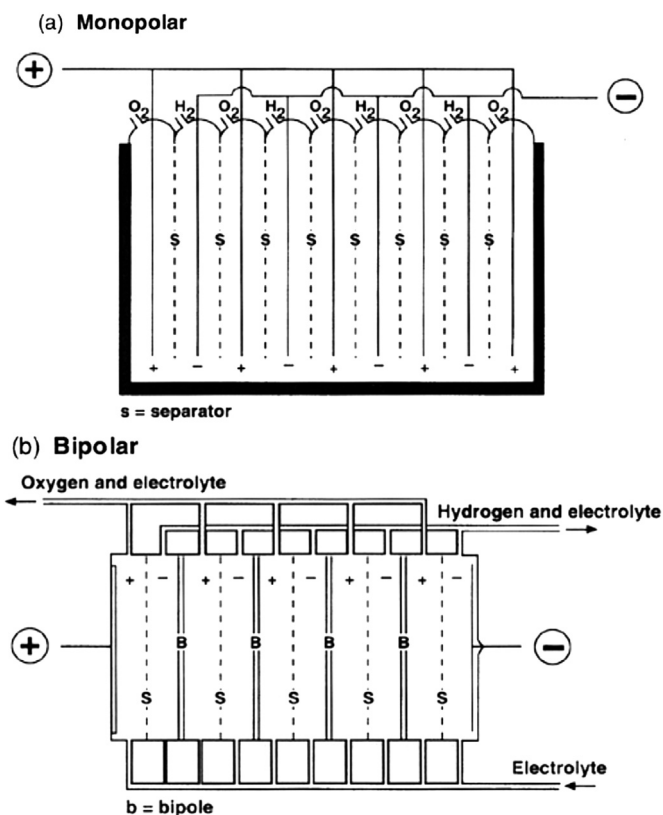
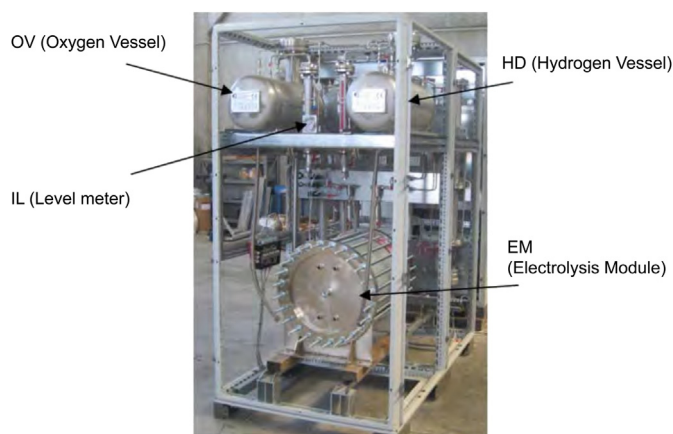


Fig. 2. Monopolar (a) and bipolar (b) design of an alkaline electrolysis cell [42].

A power conditioning system, a water purification system (usually based on reverse osmosis) and a downstream purification section (required in the case of very high purity requirements) complete the balance of the plant, as shown in the next section. Depending on the operating pressure of the electrolyzer, a compressor can be required to obtain a pressurized hydrogen flow suitable for storage or other downstream utilization. High pressure electrolysis is studied to decrease the compressor consumption; for instance in [24], the operation of a 25 bar 100 kW electrolyzer for more than 5000 h is reported. The responses of the main system parameters during operation are described; at partial load, the normally increasing hydrogen percentage in the produced oxygen is stabilized by a special circulation system.

Efforts are being made to produce highly pressurized electrolyzers to increase overall energy efficiency by eliminating mechanical compression, despite practical considerations such as corrosion, hydrogen embrittlement, operational complexity,



**Fig. 3.** Main components of the electrolyzer experimented at Politecnico di Milano—Department of Energy.

dynamic response and costs being less favorable for pressurized electrolyzers. A first study, developed by Roy [22], shows a comparison of total energy consumption at various operating pressures (up to 700 bar), which finds that atmospheric electrolyzers can be more efficient. On the other hand, in the work by Hammoudi et al. [25] pressurized systems of up to 70 bar are simulated, finding total energy consumptions (including both electrolysis and compression). The obtained results are very similar for both the pressurized and the equivalent atmospheric system in conditions near the optimal temperature, while at lower temperatures the pressurized system shows better performances. A third work by Onda [26] estimates the power required to produce high-pressure hydrogen to be about 5% less than that required for atmospheric electrolysis. Nevertheless, in any case the influence of the balance of the plant is very relevant and requires a detailed case-by-case evaluation; generally speaking, it can be said that presently the pressurized technology results show that it is particularly suitable for medium-pressure (up to 25–100 bar) and small production volumes (e.g. up to  $100 \text{ Nm}_3\text{H}_2/\text{h}$ ), although it requires improvement in terms of reliability and durability.

A mathematical model for an advanced alkaline electrolyzer is presented in [27]. The model is based on a combination of fundamental thermodynamics, heat transfer theory, and empirical electrochemical relationships. The number of required parameters has been reduced to a minimum to make the model suitable for use in integrated hydrogen energy system simulations.

In Ref. [28] a critical review of the current data on the specific conductivity of aqueous potassium hydroxide (KOH) solutions is presented. Based on this review, the empirical correlation was developed over a molarity range of 0–12 at temperatures of 0–100 °C.

The increase in electrolysis temperature was investigated in Ref. [29] and it was found that efficiency, defined by a higher heating value of the produced hydrogen (HHV) divided by the total energy of the heat and the electricity required to produce the hydrogen, above 75% (1000 °C) can be obtained (with a share between heat and electricity of about 20%–80%) — compared with an efficiency level of 47–82% with conventional alkaline solution electrolysis at lower temperatures.

Thermal performance of a commercial alkaline water electrolyzer—experimental study and mathematical modeling is presented in Ref. [30]. In this paper a study of the thermal performance of a commercial alkaline water electrolyzer designed for a rated hydrogen production of  $1 \text{ Nm}_3\text{H}_2/\text{h}$  at an overall power consumption of  $4.90 \text{ kWh/Nm}_3\text{H}_2$  is obtained.

In Ref. [31] experimental work involving the direct-current electrolysis of highly concentrated potassium hydroxide solutions at high temperatures (up to 400 °C) and under various pressures is described. The advantages of operating an alkaline electrolysis cell at high temperatures include increasing the ionic conductivity of the electrolyte and enhancing the rates of electrochemical reactions at the electrode surfaces. Cell operation with increasing steam partial pressure over the solution is also shown to enhance cell performance. The best cell performance was achieved using a cobalt-plated nickel anode at a temperature of 400 °C and a steam partial pressure of 87 bar.

Recent progress in alkaline water electrolysis for hydrogen production and applications is presented in Ref. [32]. The paper examined the fundamentals of water electrolysis, compared the performance of various water electrolysis designs and introduced several emergent water electrolysis technologies.

A new multi-physics approach for modeling and design of alkaline electrolyzers is given in Ref. [25]. The positive impact of temperature on the power consumed by the electrolyzer, the rate of hydrogen production and energy efficiency is indicated. According to this model, increasing the operating pressure induces a reduction in the power consumed by the electrolyzer and the rate of hydrogen production by a factor depending on relative pressure and temperature.

The electrical behavior of a commercial advanced alkaline water electrolyzer is investigated in Ref. [33]. The paper contains a model based on the thermodynamic, activation, double-layer and ohmic effects and phenomena that take place in a real alkaline electrolysis process. The parameters of the model are experimentally determined from both static and dynamic operating tests on the electrolyzer. The model was implemented in a MATLAB-Simulink environment and validated in three different operating conditions.

According to the literature, the available models are not generalized and are typically non-predictive, so they do not allow one to shape the design and detailed prediction of electrolyzer behavior. In this work a classical mathematical model proposed in the literature is compared with an alternative one, based on a reduced-order equivalent electric circuit and a lumped model description of the phenomena involved, as described below.

## 2. Experimental setup

Experimental investigation was performed to measure the performance of an Alkaline Electrolyzer Cell (AEC) stack built for hydrogen and oxygen generation and installed at the Laboratory of Micro-cogeneration (LMC) at Politecnico di Milano [4].

The AEC was manufactured by H2Nitidor Srl for SAPIO SpA and experimented on for a trial period—see Fig. 4 for details. The AEC works at 30 bar and has a planar area of  $500 \text{ cm}^2$  and a maximum hydrogen production of  $6.6 \text{ Nm}_3/\text{h}$ , the anode and cathode (bipolar design) are based on a solid Ni structure with thickness of 0.3 mm, and the electrolyte is a potassium hydroxide and water mixture (usually 8 M KOH), operating with a total gap between the electrodes of about 14 mm. A diaphragm is placed between the two opposing separator plates and the hydrogen and oxygen are generated in the opposing channels. The cathodic and anodic current collectors are made by a Ni mesh. The cell was tested in the experimental facility shown in Fig. 3, where the stack is held in a supporting frame and it was possible to set up and control each operating parameter. The surface liquid indicator enables measurement and control of the water directed to the electrolyte.

A proprietary control system continuously monitors through thermocouples (PT-100 type) the temperatures in stack inlet/outlet flows as well as in various positions, allowing one to easily view and control the operating condition and performances of the unit. A

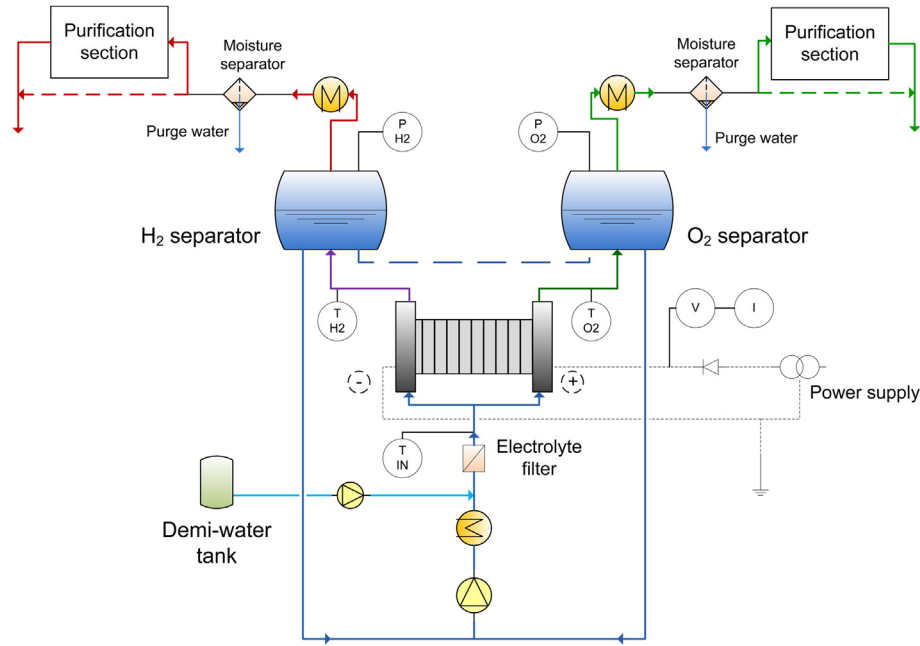


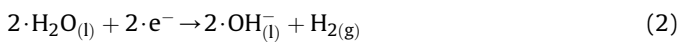
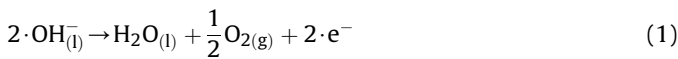
Fig. 4. Simplified scheme of the electrolyzer components and of the instrumentation.

nominal DC current of 144 A is generated by a power system based on a rectifier and a 400/180 V transformer, with nominal power 45 kW, and directly applied at the electrodes.

For the purpose of this work, experimentation consisted in collecting voltage–current curves during operation of the unit, which were later used for model validation. The accuracy of the voltage and current measurements was within  $\pm 1\%$  of the reading.

### 3. Model definition

Water electrolysis consists in the molecular decomposition by means of an externally applied direct electric current, through the anodic and cathodic reactions:



as shown in Fig. 5.

In this paper, two different modeling approaches are discussed. A common feature is the description of ionic conductivity of the cell structure, which can be split among the contributions of the layers that constitute the cell itself: the electrolyte, which is the primary ion conductor, sandwiched by anode and cathode layers that influence ionic conductivity as well as due to the triple boundary phase processes occurring at the electrolyte interface. The material used, porosity and design of the electrodes affect cell voltage significantly; as a consequence, the total ionic resistance of the cell is a function of many parameters. Additionally, electrodes can be built as multi-layers by themselves. Thus, the total ionic resistance of the AEC can be estimated by the following relationship:

$$r = \frac{\delta_{\text{KOH}}}{\sigma_{\text{KOH}}} + r_{\text{other}} \quad (3)$$

where the first term is related to the electrolyte:  $\sigma$  is the ionic conductivity and  $\delta$  the thickness of the electrolyte layer. All other effects, depending on thicknesses and conductivities of the

electrodes, can be conglomerated for simplicity in a single value of  $r_{\text{other}}$ .

Within the first term, the ionic conductivity of the alkaline solution as a function of electrolyte temperature and composition is relatively well known [28]. Fig. 6 presents the expected conductivity variation according to literature [28], which can be expressed by the following equation:

$$\sigma = -2.041 \cdot M - 0.0028 \cdot M^2 + 0.001043 \cdot M^3 + 0.005332 \cdot M \cdot T + 207.2 \frac{M}{T} - 0.0000003 \cdot M^2 \cdot T^2 \quad (4)$$

where:  $M$  — molarity,  $\text{mol l}^{-1}$ ;  $T$  — temperature, K.

Eq. (4) is plotted in Fig. 6; it should be noted that this correlation is not valid above a molarity value of 12. To extend the range of function utilization we derived a new correlation, reproducing the same results at lower molarity:

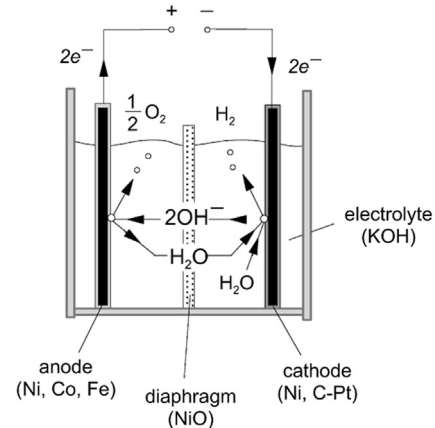


Fig. 5. Operation principle of alkaline water electrolysis [27].



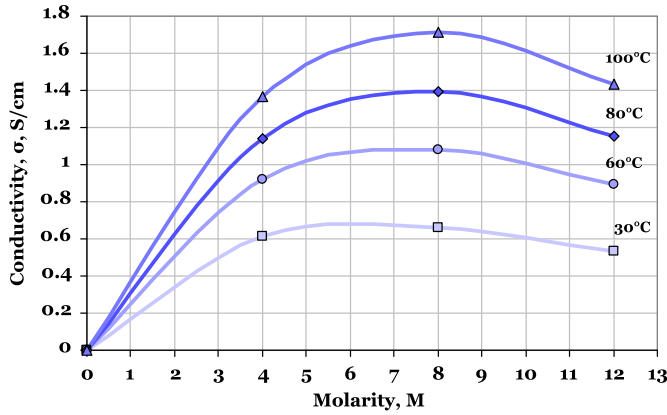


Fig. 6. Temperature and composition dependencies of ionic conductivity for KOH solution.

$$\sigma = \frac{132.1}{\exp\left(0.01592 \cdot (M - 12.27)^2 + \frac{0.3819 \cdot M + 9.406}{R \cdot T}\right)} \quad (5)$$

Eq. (5) is obtained based on the same experimental data as for Eq. (4), but it is structured with an exponential (Arrhenius type) form instead of a polynomial interpolation; it allows predicting physically consistent results for molarities greater than 12.

### 3.1. Loss-estimate approach for modeling of AEC

A complete description of the phenomena involved in alkaline electrolysis would require a multi-physics approach including different domains. The model proposed by Hammoudi in his work [25] can be taken as a reference because of its completeness and high level of detail. Alternatively, the classical simplified approach to electrochemical devices modeling describes the behavior of the system by means of a voltage–current polarization curve. The curve is obtained as a sum of contributions related to various physical phenomena, and the fundamental equations included in the model usually describe the thermodynamics of the system, the kinetics of the electrochemical reaction and the losses in the electrical equivalent circuit. This approach can be applied to both fuel cell and electrolyzer modeling, but this work is focused on alkaline technology and, therefore, the model is adapted in order to describe the particular characteristics of this device. Generally speaking, the polarization curve is described by the equation:

$$E = E_{\text{rev}} + E_{\text{act}}(i) + E_{\text{ohm}}(i) \quad (6)$$

where the three voltage contributions are respectively the ideal reversible voltage, the overvoltage due to electrochemical kinetics and the one related with electrical losses.

#### 3.1.1. Standard potential

Reversible potential can be calculated from the thermodynamics of the water dissociation reaction, considering an ideal electrolysis cell at standard temperature and pressure conditions. It can be formulated as:

$$nFE_{t,p}^{\text{rev}} = -\Delta G_{t,p} = nFE_{t,p0}^{\text{rev}} + RT \ln \left[ (p - p_w)^{1.5} \frac{p_w^*}{p_w} \right] \quad (7)$$

where the temperature and pressure influences are separated in two terms.  $n$  is the number of electric charges involved in each reaction, equal to 2 in the case of water electrolysis,  $F$  is Faraday's

constant and  $G$  Gibbs free energy. Reversible potential at a given temperature and standard pressure ( $E_{t,p0}^{\text{rev}}$ ) can be calculated according to the correlation proposed by Ref. [25]

$$E_{t,p0}^{\text{rev}} = 1.50342 - 9.956 \cdot 10^{-4}T + 2.5 \cdot 10^{-7}T^2 \quad (8)$$

The last term of Eq. (7) expresses the impact of pressure on the ideal voltage, depending on the fact that gas products are in contact with electrolyte vapors next to the electrodes. The partial pressure  $p_w$  of the gaseous electrolyte solution in contact with gas products can be calculated from the partial pressure of pure water  $p_w^*$  at the same temperature [34]. A dependence of  $p_w$  on both temperature and molarity is considered, while pure water vapor pressure and molarity are only functions of temperature due to volumetric effects. Other correlations for reversible potential at standard pressure and more complex corrections are proposed in the literature (see for instance [33]), yielding results that are only slightly different from those of Eq. (7) and of the described pressure model.

#### 3.1.2. Activation losses

The second contribution in Eq. (6) is given by the activation overpotential, which includes the effects of reaction kinetics. The rate of reaction depends on temperature, the nature of the electrodes and on the composition of the electrolyte solution next to the electrodes; it can be in general expressed by Arrhenius' law and re-written in the well-known simplified formulation of the Butler-Volmer equation, valid for redox reactions in electrochemical cells:

$$i = i_0 \left[ \exp\left(\frac{\alpha_a}{RT} nFE_{\text{act}}^a\right) - \exp\left(-\frac{\alpha_c}{RT} nFE_{\text{act}}^c\right) \right] \quad (9)$$

where  $i_0$  is the current circulating at equilibrium from and to the electrodes, named “exchange current density”, and  $\alpha_{a/c}$  are “charge-transfer coefficients” which describe the share of the energy barrier between the electrodes. An accurate description of the theory related to this model can be found in Ref. [35]. For sufficiently larger values of the overpotential, the second term becomes negligible and the Butler-Volmer equation can be approximated by the Tafel law [25]:

$$E_{\text{act}}^{a/c} = 2.3026 \frac{RT}{nF\alpha_{a/c}} \log\left(\frac{i}{i_0}\right) \quad (10)$$

Exchange current density— $i_0$ —is strongly dependent on the nature of the electrodes (materials, roughness, geometry) and therefore is considered as a fitting parameter of the model. The charge-transfer coefficients  $\alpha_{a/c}$  depend linearly on temperature [36] and the following correlations can be adopted to consider the impact of temperature:

$$\begin{aligned} \alpha_a &= 0.0675 + 0.00095 \cdot T \\ \alpha_c &= 0.1175 + 0.00095 \cdot T \end{aligned} \quad (11)$$

which are valid for Ni-based electrodes [25].

#### 3.1.3. Ohmic losses

Ohm's law can be used to model electrical losses ( $E_{\text{ohm}}$ )

$$E_{\text{ohm}} = r \cdot i \quad (12)$$

where the area specific resistance  $r$  is calculated by Eq. (3).

#### 3.1.4. Other losses

Two other explicit main contributions to cell losses can be considered: the resistance of the electrolyte itself and the additional resistance given by the presence of bubbles, both in the bulk electrolyte and as a curtain over the electrodes. In addition to this,

all other resistances (i.e. due to the electrodes and the gas separation membranes) and parasitic currents dispersed through the elements of the cells without contributions to the reaction are comprised in the additional term  $r_{\text{other}}$ .

The gas bubbles produced on the surface of the electrodes form an unstable layer that induce a local increase in the electrical resistance due to the lower conductivity of the gas with respect to the electrolyte. Many approaches are proposed in the literature in order to quantify this effect, mainly proposing correlations between the additional resistance of the bubble layer and the pure electrolyte one [37]. In particular we adopt here the correlation proposed by Bruggeman [37]:

$$\frac{\sigma_e}{\sigma_0} = (1 - \varepsilon)^{1.5} \quad (13)$$

where  $\sigma_0$  and  $\sigma_e$  are respectively the electrical conductivity in bubble-free electrolyte and in presence of bubbles.  $\varepsilon$  is the void fraction in the electrolyte that can be estimated as

$$\varepsilon = \frac{2}{3} \theta = 0.0153 \left( \frac{i}{i_{\text{lim}}} \right)^{0.3} \quad (14)$$

according to [38]. A suggested value for the limiting current density  $i_{\text{lim}}$  is  $300 \text{ kA m}^{-2}$  [39], that gives a satisfactory correlation for the experimental points reported by Ref. [38]. Note that the original Bruggeman theory, derived for effective conductivity in multicomponent systems, has already been applied to liquid electrolytes with internal void fraction [37], similarly to our case, as validated by other literature works [38]. This is a rough empirical estimation of a complex phenomenon, but is quite accurate for a lumped model.

An example of the share of the various overpotentials is shown in Fig. 7.

Concentration losses due to consumption of reactants and mass flow rate limitation towards the reactive sites, which usually play an important role in fuel cell analysis, do not have here a significant impact on performances. In fact, the whole cell is filled with the electrolyte solution, which contains liquid water with a very large excess with respect to the quantity consumed by the reaction. Therefore mass transport limitations can be neglected. The only negative dilution effect could come from the formation of gaseous products, but it is taken into account by the part of the model which deals with the presence of bubbles, which reduces the effective electrode surface and the useful section for ion conduction, as described above.

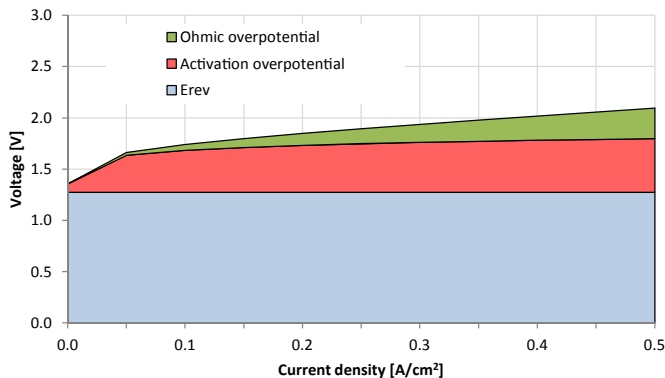


Fig. 7. Example of overvoltages share ( $T = 70^\circ\text{C}$ ,  $p = 30 \text{ bar}$ ) obtained by the loss-estimate model with fitting parameters in 1.

### 3.2. Reduced-order approach for modeling of AEC

With the reduced-order approach, the main processes occurring during electrolyzer operation can be described by the flows of ions ( $\text{OH}^-$ ) and electrons through an adequate equivalent electric circuit of the electrolysis cell, as indicated in Fig. 8. Making reference to the figure, the total current  $i_3$  is imposed on the electrolyzer by an external power supply, where the current source (DC) has its own resistivity ( $r_{\text{DC}}$ ); then the current is divided into two circuits, the first one indicated as  $i_1$  is the total electron flow transported by alkaline ions ( $\text{OH}^-$ ), whereas  $i_2$  indicates electrons which pass through the electrolyte in the same direction as the alkaline ions due to the presence of a small but significant electronic (electric) conductivity.

The current  $i_2$  could be neglected for low water utilization factors, which would simplify the model but result in an underestimation of the voltage yield  $E_{\text{OCV}} = E_{\text{ideal}}$ , where  $E_{\text{OCV}}$  is an open circuit voltage (no electric current applied). Based on the available experimental data, the value of  $i_2$  can be very easily found by a fitting procedure. During the calculation the value of  $i_2$  can be kept at a constant value. Applying Ohm's and Kirchhoff's laws to the electric circuit shown in Fig. 8, it is possible to write the following set of equations:

$$\begin{cases} E_{\text{AEC}} = r_2 \cdot i_2 \\ i_3 = i_1 + i_2 \\ E_{\text{ideal}} + i_1 \cdot r_1 = r_2 \cdot i_2 \end{cases} \quad (15)$$

The total current which can be used for water decomposition is correlated to the amount of demineralized water delivered to the electrolyte as primary reactant, which must be subject to electrolysis. Assuming the delivered water is utilized completely, the value of maximum current that must be applied  $-i_{\text{max}}$  is defined by the following relationship:

$$i_{\text{max}} \cdot A = 2 \cdot F \cdot \dot{n}_{\text{H}_2\text{O}} \quad (16)$$

where  $F$  is Faraday's constant;  $A$  is the cell area and  $\dot{n}_{\text{H}_2\text{O}}$  is the water molar flow at electrolyte inlet; all currents are expressed in terms of current densities ( $\text{A cm}^{-2}$ ) referred to the total cell area.

Hence, the water utilization factor can be correlated with the total current applied to the electrolyzer through the following relation:

$$i_3 = \eta_w \cdot (i_{\text{max}} + i_2) \quad (17)$$

where  $\eta_w$  is the water utilization factor.

By solving both Eq. (15) and Eq. (17), an equation for electrolyzer voltage is obtained:

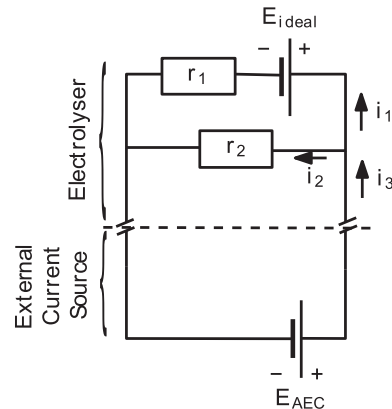


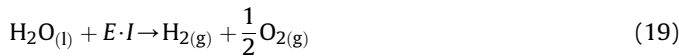
Fig. 8. Equivalent electric circuit of an electrolyzer.

$$E_{AEC} = \frac{E_{ideal} + \eta_w \cdot i_{max} \cdot T_1}{\frac{T_1}{T_2} \cdot (1 - \eta_w) + 1} + E_{DC} \quad (18)$$

Eq. (18) is the main relationship of the proposed model. AEC voltage is described by a few factors which have clear physical explanations:  $E_{ideal}$ —ideal voltage defined by the maximum work required for an isothermal process of water hydrolysis (see next chapter);  $\eta_w$ —water utilization factor defined by current working conditions of the electrolyzer;  $i_{max}$ —maximum current density defined by the quantity of delivered water;  $r_1$ —area specific internal ionic resistance (ASIR) defined by the overall ‘permeability’ of the electrolyte + electrodes structure to alkaline ions; and  $r_2$ —area specific internal electronic resistance (ASIER) defined by electric conductivity of the electrolyte, intended as the KOH solution permeating the electrolysis cell components. The compact expression of AEC voltage makes it possible to clarify how the development of the specific components of the electrolysis cell (e.g. R&D on new electrolyte compositions, new catalyst layer, etc.) should be related to optimizing the resistance factors of Eq. (18), yielding additional information with respect to the classical approach focused on optimizing the complex loss effects which contribute to the current density–voltage curve. In other words, the reduced-order equivalent circuit approach may facilitate a parallel and easier interpretation of cell behavior.

### 3.2.1. Ideal voltage for the main chemical reaction of water decomposition

The overall process occurring in the electrolysis cell includes a change of phase of the reactant (liquid water) in addition to splitting the water molecules into hydrogen and oxygen. The process can be summarized as follows, where  $E$  [V] is the voltage applied to obtain electrolysis and  $I$  [C mol<sup>−1</sup>] is the current consumed, supplying power to sustain water splitting:



The actual process of an AEC does not involve separate introduction of heat and electricity. All energy required is supplied through the electrical current, and the minimum voltage required to sustain the overall process can be calculated as:

$$E_{ideal} = \frac{R \cdot T}{2 \cdot F} \ln K + \frac{R \cdot T}{2 \cdot F} \ln \frac{p_{H_2} \cdot p_{O_2}^{\frac{1}{2}}}{p_{H_2O} \cdot p_{ref}^{\frac{1}{2}}} + \frac{Q}{2 \cdot F} \quad (20)$$

where:  $R$ —universal gas constant,  $F$ —Faraday’s constant [C mol<sup>−1</sup>],  $p$ —partial pressure [Pa], ref—reference,  $K$ —chemical equilibrium constant (calculated with outlet concentrations),  $Q$ —water evaporation heat,  $Q = f(T)$  [J mol<sup>−1</sup>] [40]:

$$Q = -5 \cdot 10^{-6} \cdot (T - 273.15)^4 + 0.0024 \cdot (T - 273.15)^3 - 0.4867 \cdot (T - 273.15)^2 - 11.927 \cdot (T - 273.15) + 44714 \quad (21)$$

It should be noted that the Nernst equation is referred to the partial pressures of reactants in the gaseous state (e.g. at the outlet), although water is delivered as a liquid. Accordingly, an additional term regarding the energy required for water evaporation ( $Q$ ) must be included in the equation. Expression for calculating  $E_{ideal}$  is quite complex as can be seen in Fig. 9; the contribution given by evaporation heat is evident and causes the step in the ideal voltage curve. Assuming standard conditions ( $p = 1$  atm,  $T = 25$  °C), the reversible potential  $E_{ideal}$  is 1.229 V.

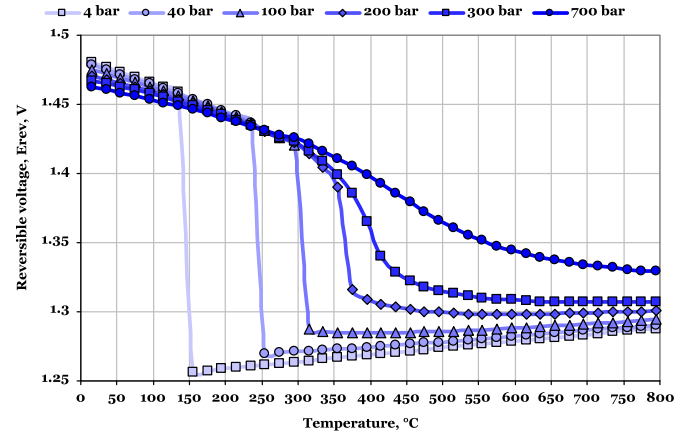


Fig. 9. Influence of pressure and temperature on the value of reversible electrolysis voltage calculated following Eq. (20).

Thus, partial pressures of hydrogen, oxygen and water vapor should be put into Eq. (20). Hydrogen and oxygen pressure values are quite obvious, since they correspond to the pressure of the gases during electrolyzer operation—if there is no pressure losses—produced and stored gases, which is equal to the operating pressure of the electrolyte (varying by adequate humidity of the gases). For water vapor, the partial pressure can be defined in terms of hydrogen/oxygen purity. Here we assume that the water content in the hydrogen and oxygen flows corresponds to the saturation line, i.e. 100% of relative humidity for a given temperature of the electrolyte, according to the following equation [40]:

$$p_{H_2O} = 1.508 \cdot 10^{-8} \cdot (T - 273.15)^4 - 2.033 \cdot 10^{-6} \cdot (T - 273.15)^3 + 2.425 \cdot 10^{-4} \cdot (T - 273.15)^2 - 0.01105 \cdot (T - 273.15) + 0.2118$$

### 3.2.2. Maximum current density— $i_{max}$

In the proposed model,  $i_{max}$  can be an assumption or a result depending on the considered approach, namely a “design-point” or an “off-design” modeling of the electrolyzer. During “design-point” modeling, the cell area can be changed depending on the nominal inlet water flow and according to the optimization of other design parameters (electrolyte type, distance between electrodes, etc.), including the maximum current density  $i_{max}$ . The value of  $i_{max}$  is then the result of a technical-economic optimization: the lower the value the larger the cell area of the electrolyzer for the same water utilization factor, with higher investment costs. An example could be  $i_{max} = 4$  A cm<sup>−2</sup>, a reasonable value based on the researchers’ own calculations and data taken from previous experiments. Since the value of maximum current density is assumed after the optimization process, instead of a voltage–current density curve ( $E = f(i)$ ) the voltage–water utilization factor curve ( $E = f(\eta_w)$ ) can be assumed as an electrolyzer characteristic curve.

The typical “off-design” behavior of the cell is instead commonly defined by a voltage–current density curve ( $E = f(i)$ ), and in this case the area of the cell is a fixed parameter, while reactant flow parameters can be changed. Hence factor  $i_{max}$  has to be calculated using Eq. (16), depending on the actual water flow delivered to the electrolyzer and the assumed active area of the electrolyzer. This approach makes it possible to compare various cells with different areas. Actually,  $i_{max}$  is assumed as the maximum current that should be consumed by the electrolyzer to convert all make-up water into hydrogen and oxygen.

### 3.2.3. Ionic and electric resistances

Total ionic resistance of the cell  $r_1$  is calculated using Eq. (3) and  $r_{\text{other}}$  is in the end a fitting parameter of the model.

Existence of  $r_2$  (electronic resistance of the cell) means that some electric current flows through the cell itself without participating in water decomposition and without being visible externally. Thus, the water utilization factor defined by Eq. (17) is not the real value of water decomposed due to  $r_2$ . The real value of water utilization factor can be defined by the following function:

$$\eta_{w,\text{real}} = \eta_w - E_{\text{AEC}} \cdot \frac{1 - \eta_w}{r_2 \cdot i_{\text{max}}} \quad (22)$$

In practice both values are very close to each other and the discussion is largely theoretical; nevertheless it should be noted that there is a limiting value of  $\eta_w$  for which there is no real water utilization.

## 4. Model calibration and validation

Both presented models were calibrated based on the same set of experimental data, obtained by the AEC unit described above in Section 2. The main parameters of the model are listed in Table 1.

While volumetric (molar) flow rate for hydrogen is double than for oxygen, output flows from the AEC unit are controlled so that total pressure is more or less the same for oxygen and hydrogen after the system is pressurized and the separation tanks (see Fig. 4) are filled in up to the rated output pressure. All the fitting parameters were selected based on feasible ranges obtained from the literature, and calibrated to best fit the experimental results (for instance, electrolyte resistance of  $300 \text{ cm}^2 \text{ S}^{-1}$  is compatible with conductivity values given in Ref. [41] for aqueous solutions). It turned out for both approaches the possibility to correctly predict the cell behavior, validating their physical sense. The reduced-order model contains two fitting parameters:

- area specific internal electric resistance of the electrolyte  $r_2$
- electrodes losses  $r_{\text{other}}$  (which added to the electrolyte ionic resistance yields  $r_1$ , see Eq. (3)).

On the other hand, the loss-estimate model contains the following five fitting parameters:

- exchange current  $i_0$
- anode and cathode charge-transfer coefficient  $\alpha_a$  and  $\alpha_c$
- limiting current density in void fraction estimation  $i_{\text{lim}}$
- coefficient for bubble coverage of electrodes (see Eq. (14))

**Table 1**  
Main parameter of the two proposed models.

Parameter	Value	
	RO model	LE model
Temperature, °C	70	70
Electrolyte thickness, cm	0.66	0.66
Electrolyte specific flow, $\text{ml cm}^{-2} \text{ h}$	1.5	—
Hydrogen pressure, bar	25	25
Oxygen pressure, bar	23	—
Other (e.g. electrodes) resistance, $\text{cm}^2 \text{ S}^{-1}$	0.96 <sup>a</sup>	—
Electrolyte electric resistance, $\text{cm}^2 \text{ S}^{-1}$	300 <sup>a</sup>	—
Exchange current density, $i_0$ , $\text{A cm}^{-2}$	—	$3.15 \cdot 10^{-4a}$
Anode charge-transfer coefficient, $\alpha_a$	—	0.39 <sup>a</sup>
Cathode charge-transfer coefficient, $\alpha_c$	—	0.44 <sup>a</sup>
Limiting current density, $i_{\text{lim}}$ , $\text{A cm}^{-2}$	—	30 <sup>a</sup>
Bubbles coverage coefficient	—	0.0153 <sup>a</sup>
Inlet electrolyte molarity, M ( $\text{mol KOH/l}$ )	8	8

<sup>a</sup> Fitting parameter or literature correlation.

These parameters are related with electrochemical behavior (Tafel equation) and with resistive effects due to bubbles. A comparison between the models and the experimental data is shown in Fig. 10.

After the fitting procedure, both models give similar errors with average deviation of below 3% with respect to the experimental data, a reasonably low value which is also not too far from measurement accuracy in typical applications.

The relevant difference in the results given by the two described approaches is the behavior at very low current density values; in Fig. 10 the curves are extended in the low current field in order to show this effect. The reduced-order model maintains its almost linear trend whereas the loss-estimate model shows a drop in voltage due to the non-linear description of the electrochemical kinetics. As a consequence, the predicted “open circuit” voltage of the cell results are very different. In common operation of electrolysis alkaline units this issue is not very important, because the lower power limit for continuous operation is set at around 20%, i.e. above the region where the two models differ. Nevertheless, further experimental investigations at low current densities could be useful in terms of validating the proposed models and studying an extension of the operating range of the units.

The obtained experiment results were also compared against other literature data for the same AEC operating temperature (see Fig. 11). Although the polarization curves have the same tendency, the comparison showed that the data obtained during experiments shifted slightly above ( $\approx 0.11 \text{ V}$ ) other literature data, evidencing that the experimented unit was affected by higher electrical losses than the average literature references. This mismatch can be also a result of the relatively large gap (14 mm) between the electrodes of the electrolyzer under consideration. Nevertheless, this could be the effect of an intrinsic different internal design of the cells. Due to an interruption of the experimental investigation for maintenance on the AEC unit, this issue was not investigated further, but future planned experimental investigations will focus on this aspect as well.

As a concluding remark, it can be said that from a general point of view, both of the discussed models can reproduce rather accurately the voltage–current density curve of an alkaline electrolyzer. Thus, the reduced-order approach is an efficient alternative to the more established loss-estimate approach currently proposed in literature, and may be applied with the advantage of requiring a lower number of parameters (mainly easily measurable), whereas the parameters of the electrochemical description in the loss-estimate model are based on correlations that are strongly dependent on the nature of electrode materials and on local electrochemical and fluid-dynamic conditions. On the other hand, with

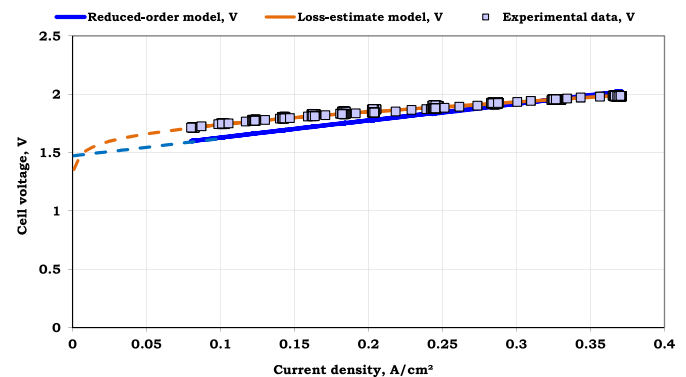


**Fig. 10.** Results of the models validation. Average error on level of 2.5% for reduced-order model and of 1.5% for loss-estimate model.



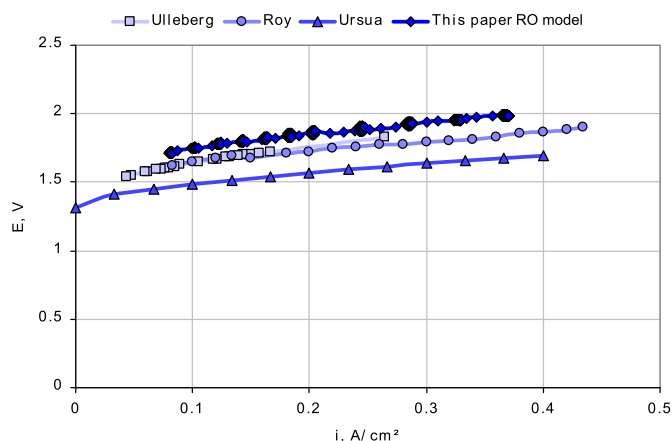


Fig. 11. Comparison of polarization curves taken from available literature [22,27,33] (operating temperature at  $\approx 70^\circ\text{C}$ ) against data obtained during experiments.

respect to the geometric design purpose, both proposed approaches are limited since they neglect the real distribution of the reactant and products between the cell layers; thus, any optimization of the cell geometry would be based only on its electrical effects, neglecting analysis of relevant internal mass transfer phenomena.

## 5. Conclusions

This work presents two approaches to the modeling of Alkaline Electrolyzers: the first based on a classic loss-estimate, requiring calibration of specific parameters related to the electrochemical and thermophysical behavior of the cell (e.g. activation losses, bubble coverage effects, transport phenomena), the second based on a reduced-order equivalent circuit approach, decoupled from the fundamental physical phenomena which occur in the electrochemical cell.

Based on the results of experiments on a real electrolyzer carried out at Politecnico di Milano, both models show a capacity to describe the general behavior of an electrolysis device and fitting on a specific device with sufficiently accurate results (average error below 3% after fitting of model parameters), which are quite similar for the two approaches. They differ just in the very low current density zone, which is generally not interesting for practical applications due to safety and control issues. In both cases the number of required parameters was reduced to the minimum and the models are suitable for use in complex hydrogen energy system simulations. Therefore the evaluation of an equivalent electrical circuit or reduced-order lumped description of the phenomena involved makes for an interesting alternative to the classical approach. Further investigations should focus on the application of this approach to unsteady modeling of electrolyzers and coupling with intermittent energy sources.

## Acknowledgment

Work co-financed by Didactic Development Program for Faculty of Power and Aeronautical Engineering from the European Social Fund Operational Programme Human Capital (POKL04.01.01-00-

061/10). We acknowledge and are grateful to SAPIO and H2Nitidor for the support in the experimental investigation activity.

## References

- [1] EG&G.TechnicalServices, Fuel Cell Handbook, Tech. rep, seventh ed., DOE, 2004.
- [2] W. Budzianowski, Rynek Energii 95 (4) (2011) 127–133.
- [3] J. Kupecki, K. Badyda, Soft-based micro-chp system as an example of efficient power generation unit, Archives Thermodyn. 32 (3) (2011) 33–43.
- [4] S. Campanari, G. Valenti, E. Macchi, G. Lozza, N. Ravidà, Appl. Therm. Eng. Available online 8 November 2013, ISSN: 1359–4311, doi:10.1016/j.applthermaleng.2013.10.067.
- [5] McKinsey, The Role of Battery Electric Vehicles, Plug-in Hybrids and Fuel Cell Electric Vehicles, Tech. rep., 2010 www.zeroemissionvehicles.eu
- [6] P. Costamagna, S. Srinivasan, J. Power Sources 102 (1–2) (2001) 253–269.
- [7] H. Zhang, P. Shen, Chem. Rev. 112 (5) (2012) 2780–2832.
- [8] S. Singhal, K. Kendall, High Temperature Solid Oxide Fuel Cells: Fundamentals, Design and Applications, Elsevier, 2003.
- [9] K. Huang, J.B. Goodenough, Solid Oxide Fuel Cell Technology, Woodhead Publishing - CRC Press, 2009.
- [10] J.-H. Wee, Appl. Energy 88 (12) (2011) 4252–4263.
- [11] A. Kulkarni, S. Giddey, J. Solid State Electrochem. 16 (10) (2012) 3123–3146.
- [12] L. Blum, R. Deja, R. Peters, D. Stolten, Int. J. Hydrogen Energy 36 (17) (2011) 11056–11067.
- [13] F. Díaz-González, A. Sumper, O. Gomis-Bellmunt, R. Villafañila-Robles, Renew. Sustain. Energy Rev. 16 (4) (2012) 2154–2171.
- [14] L. Aline, Hydrogen Technology, Springer, 2008.
- [15] W. Kreuter, H. Hofmann, Int. J. Hydrogen Energy 23 (8) (1998) 661–666.
- [16] G. Guandalini, S. Campanari, M.C. Romano, Comparison of gas turbines and power-to-gas plants for improved wind park energy dispatchability, in: Proc. Of ASME Turbo Expo 2014, 2014, pp. GT2014–26838.
- [17] M. Carmo, D. Fritz, J. Mergel, D. Stolten, Int. J. Hydrogen Energy 38 (12) (2013) 4901–4934.
- [18] V. Di Noto, S. Lavina, G. Giffin, E. Negro, B. Scrosati, Electrochim. Acta 57 (1) (2011) 4–13.
- [19] M. Laguna-Bercero, J. Power Sources 203 (2012) 4–16.
- [20] M. Ni, M. Leung, D. Leung, Int. J. Hydrogen Energy 33 (9) (2008) 2337–2354.
- [21] J. Stempien, Q. Sun, S. Chan, Energy 55 (2013) 647–657.
- [22] A. Roy, S. Watson, D. Infield, Int. J. Hydrogen Energy 31 (14) (2006) 1964–1979.
- [23] A. Ursua, L.M. Gandia, P. Sanchis, Proc. IEEE 100 (2) (2012) 410–426 id: 1.
- [24] C. Schug, Int. J. Hydrogen Energy 23 (12) (1998) 1113–1120.
- [25] M. Hammoudi, C. Henao, K. Agbossou, Y. Dubé, M. Dombia, Int. J. Hydrogen Energy 37 (19) (2012) 13895–13913.
- [26] K. Onda, T. Kyakuno, K. Hattori, K. Ito, J. Power Sources 132 (1–2) (2004) 64–70.
- [27] O. Ulleberg, Int. J. Hydrogen Energy 28 (1) (2003) 21–33.
- [28] R. Gilliam, J. Graydon, D. Kirk, S. Thorpe, Int. J. Hydrogen Energy 32 (3) (2007) 359–364.
- [29] Y. Shin, W. Park, J. Chang, J. Park, Int. J. Hydrogen Energy 32 (10–11) (2007) 1486–1491.
- [30] P. Diéguez, A. Ursúa, P. Sanchis, C. Sopena, E. Guelbenzu, L. Gandía, Int. J. Hydrogen Energy 33 (24) (2008) 7338–7354.
- [31] J.C. Ganley, Int. J. Hydrogen Energy 34 (9) (2009) 3604–3611.
- [32] K. Zeng, D. Zhang, Prog. Energy Combust. Sci. 36 (3) (2010) 307–326.
- [33] A. Ursúa, P. Sanchis, Int. J. Hydrogen Energy 37 (24) (2012) 18598–18614.
- [34] R.L. LeRoy, C.T. Bowen, D.J. LeRoy, J. Electrochem. Soc. 127 (9) (1980) 1954–1962.
- [35] A.J. Bard, L.R. Faulkner, Electrochemical Methods: Fundamentals and Applications, second ed., Wiley, New York, 2001.
- [36] B.E. Conway, D.J. MacKinnon, B.V. Tilak, Transactions Faraday Soc. 66 (1970) 1203–1226.
- [37] G. Kreysa, M. Kuhn, J. Appl. Electrochem. 15 (4) (1985) 517–526.
- [38] H. Vogt, R.J. Balzer, Electrochim. Acta 50 (10) (2005) 2073–2079.
- [39] R. Piontelli, B. Mazza, P. Pedferri, A. Tognoni, Electrochim. Metall. 2 (1967) 385.
- [40] J.H. Keenan, F.G. Keyes, Thermodynamic and Transport Properties of Steam, Wiley and Sons, 1959.
- [41] D.R. Lide, CRC Handbook of Chemistry and Physics, ninetyth ed., 2009.
- [42] C.A.C. Sequeira, D.M.F. Santos, Ciência Tecnologia Dos Materiais 22 (3/4) (2010) 76–86.